# Theoretical Study of the Water Oxidation Mechanism with Non-heme Fe(Pytacn) Iron Complexes. Evidence That the Fe^{IV}(O)(Pytacn) Species Cannot React with the Water Molecule To Form the O−O Bond

Ferran Acuña-Parés, Miquel Costas, Josep M. Luis,* and Julio Lloret-Fillol*

Institut de Química Computacional i Catàlisi (IQCC) and Departament de Química, Universitat de Girona, Campus Montilivi, E-17071 Girona, Catalonia, Spain

Ⓢ *Supporting Information*

ABSTRACT: Recent studies have shown that non-heme iron complexes $[Fe(L^{N4})X_2]$, where L^{N4} stands for a tetradentate nitrogen based aminopyridine ligand (L^{N4} = Pytacn, mcp or mep, Pytacn = 1-(2-pyridylmethyl)-4,7-dimethyl-1,4,7-triaza-cyclononane, mcp = N,N'-dimethyl-N,N'-bis(2-pyridylmethyl)cyclohexane-*trans*-1,2-diamine, mep = N,N'-dimethyl-N,N'-bis(2-pyridylmethyl)ethylendiamine), and X are monodentate ligands (X = Cl, CH_3CN, $CF_3SO_3^-$, or H_2O),

catalyze the oxidation of water using cerium(IV) ammonium nitrate (CAN) as oxidant. Spectroscopic monitoring of catalytic water oxidation with $[Fe(CF_3SO_3)_2(Pytacn)]$ established $[Fe^{IV}(O)(OH_2)(Pytacn)]^{2+}$ as an intermediate along the catalytic pathway, raising the question if these high valent species could be directly responsible for the O−O bond formation event. Herein, this question is addressed by a computational analysis of the thermodynamic and kinetic parameters associated with the reaction of non-heme iron complexes $[Fe^{IV}(O)(OH)(Pytacn)]^+$, $[Fe^{IV}(O)(OH_2)(Pytacn)]^{2+}$, and $[Fe^{IV}(OH)(OH)(Pytacn)]^{2+}$ with water. Two different mechanisms have been studied for $[Fe^{IV}(O)(OH)(Pytacn)]^+$; the nucleophilic water attack assisted by the hydroxyl group as internal base, which is the lowest energy path, and the external nucleophilic water attack. For $[Fe^{IV}(OH)(OH)(Pytacn)]^{2+}$, only the attack assisted by the internal base has been studied, while in the case of $[Fe^{IV}(O)(OH_2)(Pytacn)]^{2+}$, the only viable mechanism is the external nucleophilic water attack. Up to four water molecules were needed to be included in modeling of the O−O bond formation event for a proper description of the external nucleophilic water attack. The lowest Gibbs energy barrier and reaction free energy found for the direct water nucleophilic attack to the oxo ligand are of 32.2 and 28.3 kcal·mol^{-1} for $[Fe^{IV}(O)(OH)(Pytacn)]^+$, 52.0 and 40.5 kcal·mol^{-1} for $[Fe^{IV}(O)(OH_2)(Pytacn)]^{2+}$, and 28.3 and 28.3 kcal·mol^{-1} for $[Fe^{IV}(OH)(OH)(Pytacn)]^{2+}$, respectively. These energy barriers and endergonic reaction energies are too high for the reaction to proceed and inconsistent with the relatively rapid reaction rates determined experimentally ($\Delta G^{\ddagger}_{(exp.)}$ = 17.6 kcal·mol^{-1}). Therefore, this study provides strong evidence against the O−O bond formation by these species. The energetic accessibilities of Fe^V(O) and Fe^{VI}(O) intermediates have also been investigated, showing that Fe^V is the higher oxidation state accessible under catalytic conditions, consistent with our previous results.
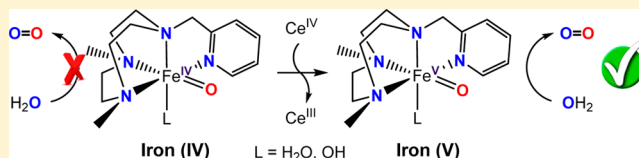
■ INTRODUCTION

The oxidation of two water molecules to form dioxygen is a highly appealing reaction because it constitutes the bottleneck for the realization of artificial photosynthesis. Water oxidation (WO) is a multielectron and multiproton uphill process that requires catalysts that could mediate the challenging O−O bond formation reaction. Nature has efficiently solved the water oxidation in the oxygen evolving center (OEC) located at photosystem II in algae and green plants.[1] The understanding of the water oxidation mechanism in the OEC could lead to the discovery of more efficient and robust water oxidation catalysts.[2]

Owing to sustainability considerations, during the last years, remarkable efforts have been directed toward the design of catalysts based on earth-abundant and inexpensive transition metals such as manganese,[3−5] cobalt,[6−10] and, more recently, iron[11,12] and copper.[13,14] In this line, the design of water oxidation catalysts (WOCs) based on iron is highly attractive because it is abundant, environmental friendly, and inexpensive.

The study of the fundamental aspects of the reactivity of well-defined iron coordination complexes in the water oxidation reaction may bring some insight into the chemistry in the natural oxygen evolving complex. Non-heme Fe^{II} complexes with tetradentate nitrogen based ligands are among the most active water oxidation catalysts based on first row transition metals described so far and that operate under homogeneous conditions.[11,12] We have previously found that, by using cerium ammonium nitrate (CAN) as a sacrificial oxidant, iron catalysts with neutral tetradentate ligands and two available *cis* positions are effective in the WO reaction in acidic conditions (pH = 1). On the contrary, neutral tetradentate ligands with *trans*-labile sites or pentadentate ligands are inactive. Experimental and theoretical results suggest that tetradentate iron complexes with *cis*-labile positions share a common catalytic cycle (Figure 1a).[12,15,16] Spectroscopic monitoring showed that the initial Fe^{II}

a)

b)
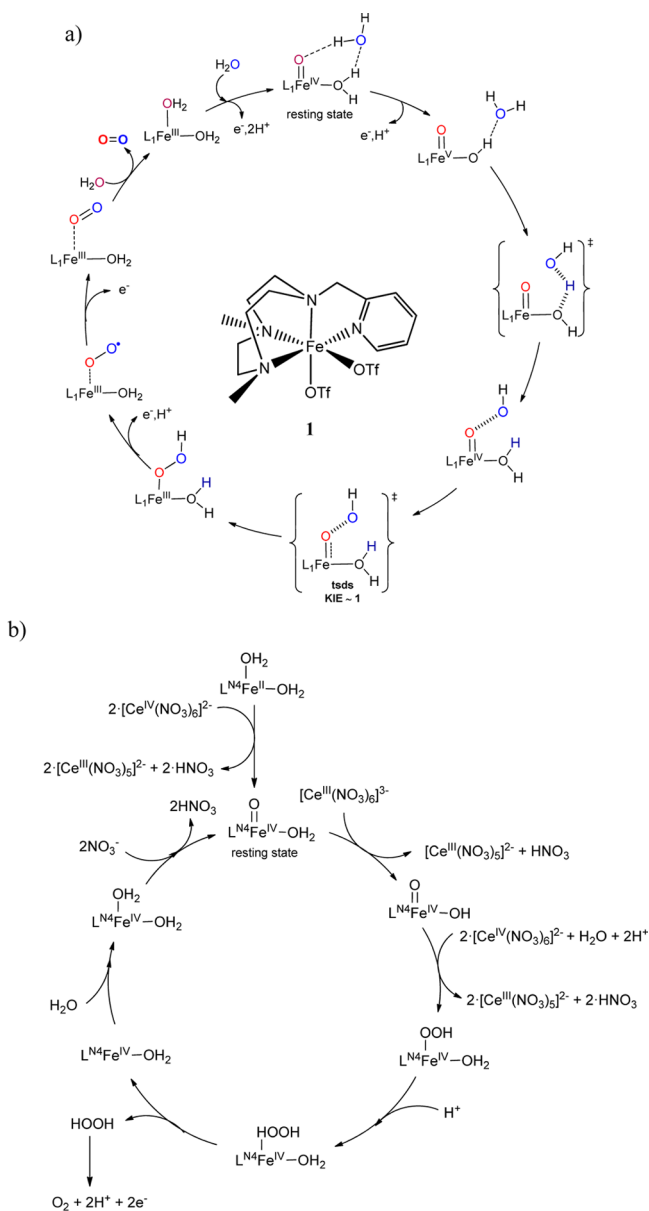
Figure 1. Proposed catalytic cycles for the water oxidation reaction catalyzed by non-heme iron complex **1**. (a) The DFT catalytic cycle involving an Fe^V intermediate previously proposed by our group.[16] (b) Theoretical proposal by Kasapbasi and co-workers which occurs exclusively at the Fe^{IV} oxidation state.[17]

complexes are immediately oxidized by the addition of a slight excess of Ce^{IV} (3 equiv at pH 1) to quantitatively form the resting state $[Fe^{IV}(O)(OH_2)(L^{N4})]^{2+}$ (L^{N4} stands for i.e. Pytacn, mcp, and mep, among others). Under these conditions, these intermediates were found to be relatively stable, with a half-life time between 20 and 200 min. Moreover, no O_2 was detected after the decay of these intermediates. At low concentrations of CAN, the reaction rate presents a first order dependence with respect to the concentration of both the metal and the sacrificial oxidant. This result excludes the possibility of a direct coupling (DC) mechanism between two Fe^{IV}=O moieties to form the O–O bond, and the WO reaction can be expected to occur at a single site. Therefore, the $[Fe^{IV}(O)(OH_2)(L^{N4})]^{2+}$ species could not be responsible for the O–O bond formation. Instead, O_2 formation was detected when an excess of CAN was added to a solution of

Scheme 1. Studied O–O Bond Formation Pathways Involving Fe^{IV} Species[a]
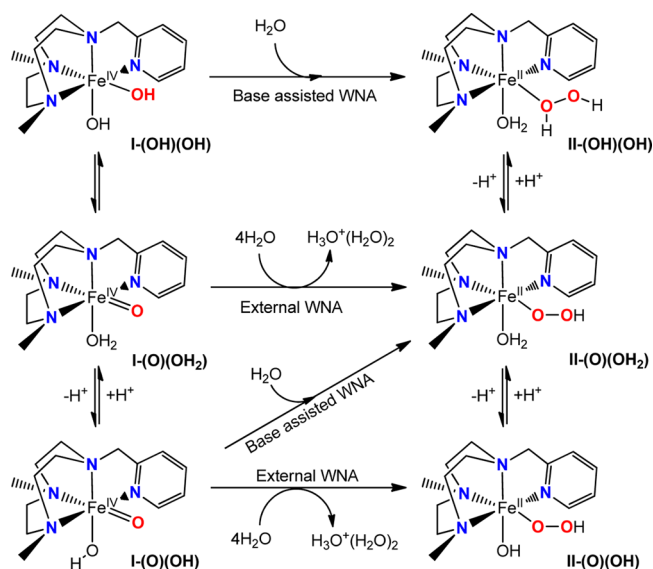
[a]The microsolvation of the iron complex was modeled by three explicit water molecules. WNA stands for Water Nucleophilic Attack.

$[Fe^{IV}(O)(OH_2)(L^{N4})]^{2+}$, which suggests that the formation of the O–O bond requires a higher oxidation state of the iron center, i.e., the $[Fe^V(O)(OH)(L^{N4})]^{2+}$ species. Density functional theory (DFT) calculations supported the accessibility of the $[Fe^V(O)(OH)(Pytacn)]^{2+}$ species under catalytic conditions. Furthermore, the DFT free energy barrier for the O–O bond formation mechanism involving the nucleophilic water molecule attack (WNA) to a highly electrophilic $[Fe^V(O)-(OH)(Pytacn)]^{2+}$ was 18.5 kcal·mol^{-1}, in very good agreement with the experimental value ($\Delta G^{\ddagger}_{(exp.)}$ = 17.6 kcal·mol^{-1}).[16] Nevertheless, there is a lack of information about the kinetics of the O–O bond formation reaction from non-heme $Fe^{IV}(O)$ species, which is the matter herein.

Closely related to our work, Kasapbasi et al. recently reported a theoretical study proposing a WO catalytic cycle accomplished by non-heme iron catalyst **1** on the basis of DFT calculations.[17] The authors suggest that all the species involved in the catalytic cycle have the same oxidation state (Fe^{IV}) and that the species driving the O–O bond formation event is the $[Fe^{IV}(O)(OH)(Pytacn)]^+$ intermediate, which is formed via deprotonation of the resting state $[Fe^{IV}(O)(OH_2)(Pytacn)]^{2+}$ (Figure 1b). The nitrate anions present in the coordination sphere of the Ce^{IV} cation are proposed to act as the base for this reaction.

Taking the proposal by Kasapbasi into consideration, in this work we sought to investigate by computational methods the competence of the spectroscopically detected $[Fe^{IV}(O)(OH_2)-(Pytacn)]^{2+}$, its isomeric form $[Fe^{IV}(OH)(OH)(Pytacn)]^{2+}$, and its conjugated base $[Fe^{IV}(O)(OH)(Pytacn)]^+$ to perform the O–O bond formation event (Scheme 1). We have also analyzed under which conditions the WO catalytic cycle proposed by Kasapbasi et al. could be viable. Finally, we have investigated the energetic accessibility of $Fe^V(O)$ and $Fe^{VI}(O)$ intermediates under catalytic conditions and their role as possible catalytic active species in the WO reaction. The key to our study is the inclusion of explicit water molecules in the computed mechanism, as well as enthalpic and entropic

corrections, which are particularly important in the estimation of the computed pK_a of the nitrate anions.

There is also the possibility that binuclear Fe^{IV} species might participate in the O—O bond formation event. For instance, Que and co-workers presented the first non-heme diiron(IV) complex with the capacity to oxidize water through formation of hydroxyl radicals via a hydrogen abstraction reaction.[18] In addition, Ray and co-workers have shown that a hexanuclear iron complex supported on a stannoxane core can undergo a facile O—O bond formation between two Fe^{IV}=O moieties, revealing the viability of a DC mechanism.[19] Moreover, the conversion of a bis-TPA peroxodiiron(III) complex to oxodiiron(IV) species via reversible O—O bond rupture was observed by the Kodera and co-workers.[20] However, kinetic studies on complex **1** revealed a first order dependence with respect to the concentration of both iron complex and sacrificial oxidant, excluding for complex **1** that the O_2 evolution occurs through a bimetallic reaction pathway.

■ COMPUTATIONAL DETAILS

All structure optimizations were performed at the DFT(B3LYP-D_2)[21−23] level with the 6-31G* basis set for all atoms and taking into account the solvent effects and the dispersion corrections. All calculations were done using Gaussian09 software.[24] Spin unrestricted B3LYP calculations were performed on all possible conformers, and all corresponding spin states for the iron metal center were taken into account to locate the ground state. The nature of the stationary points was confirmed by frequency calculations in aqueous phase, where minima have no imaginary frequencies and transition states have only one. The connectivity between minimums and transition states was confirmed through intrinsic reaction coordinate (IRC) calculations. The energies were further refined by single-point calculations with the cc-pVTZ dunning basis set for all atoms ($E_{cc\text{-}pVTZ}$). The London dispersion effects were introduced with the B3LYP-D_2 Grimme correction (E_{disp}),[25] and free energy corrections (G_{corr}), which include the enthalpic and entropic terms, were determined from gas-phase frequency calculations at the B3LYP/6-31G* level on aqueous-phase structures. The solvating effect of the aqueous medium was taken into account through the SMD polarizable continuum model (G_{solv}).[26] All calculated solvation free energies of the solute molecules were set to a standard state of an ideal gas at a gas-phase concentration of 1 mol·L^{-1} that is dissolved as an ideal dilute solution at a liquid-phase concentration of 1 mol·L^{-1}. For the explicit solvent water molecules, a 55.6 M standard state was employed. Thus, as has been indicated by Cramer et al.,[27] we calculated the free energy associated with the phase change from a standard-state gas-phase pressure of 1 atm to a standard-state gas-phase concentration of 1 M (55.6 M), $\Delta G^{\circ/*}$. The value of $\Delta G^{\circ/*}$ at 298 K is 1.9 kcal·mol^{-1} for 1 M standard-state solutes and 4.3 kcal·mol^{-1} for 55.6 M standard-state explicit water molecules. Then, the total Gibbs free energies (G) were given by

$$G = E_{cc-pVTZ} + E_{disp} + G_{corr} + G_{solv} + \Delta G^{\circ/*} \qquad (1)$$

The aqueous pK_a values are calculated using the following formula, as it was described previously:[27]

$$pK_a = \frac{\Delta G}{RT \ln(10)} \qquad (2)$$

The mean error for B3LYP calculations is around 2−4 kcal·mol^{-1},[28,29] which in the worst case translates into an error of 3 pK_a units.

Standard reduction potentials, relative to the standard normal hydrogen electrode (SHE), were calculated by

$$E^{\circ} = -\frac{\Delta G^{\circ} - \Delta G^{\circ}_{SHE}}{nF} \qquad (3)$$

where ΔG° is the free energy change associated with reduction at standard conditions, n is the number of electrons involved in the redox reaction, F is the Faraday constant, and ΔG°_{SHE} is the free energy change associated with the reduction of a proton (−4.28 eV).[30] For a proton-coupled electron transfer (PCET), where electron transfer and proton transfer to the solvent occur simultaneously, we must include in ΔG° of eq 3 the standard free energy of a proton in solution:

$$G^{H+}_{aq} = G^{H+}_{gas} + \Delta G^{H+}_{solv} + \Delta G^{\circ/*} \qquad (4)$$

where the free energy of solvation of a proton (ΔG^{H+}_{solv}) was taken from experiment as −265.9 kcal·mol^{-1},[30] and the gas-phase Gibbs free energy of a proton (G^{H+}_{gas}) is a small correction of −6.3 kcal·mol^{-1}.

The labels **I-(O)**, **TS-(O)**, **II-(O)**, and **III-(O)** were used as short nomenclature of reactants, transition states, intermediates, and products involved in the O—O bond formation event by complex **1**. The labels **a** and **b** refer to the two *cis*-tautomeric forms of complex **1**. In tautomer **a** the Fe=O moiety is in a *trans* relative position to one of the Me-substituted amines. The subscripts **s**, **t**, and **qt** are used to specify the singlet, triplet, and quintuplet spin state of the metal center, and the **H_2O** and **OH** labels are related to the nature of the *cis* ligand with respect the oxo group. Finally, the subscript **int** is used when the *cis* ligand to the oxo group acts as an internal Brønsted base.

■ RESULTS AND DISCUSSION

O—O Bond Formation Mechanism through $[Fe^{IV}(O)$-$(OH_2)(Pytacn)]^{2+}$. UV−vis, ^1H NMR spectroscopy, and

Scheme 2. O_2 Evolution and Regeneration of the $[Fe^{IV}(O)(OH_2)(Pytacn)]^{2+}$ Resting State through Hydroperoxo Intermediates
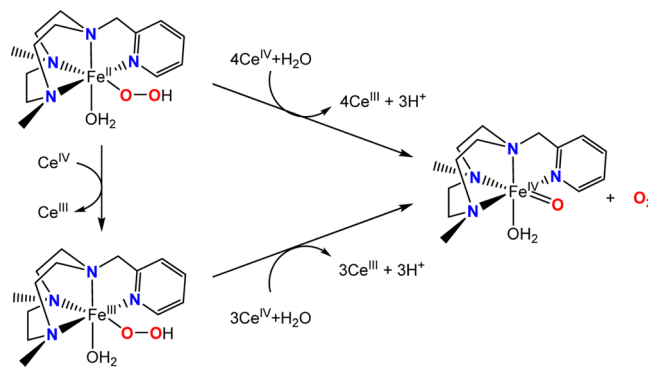
electrospray ionization mass spectrometry (ESI−MS) show that oxo-aqua Fe^{IV} species $[Fe^{IV}(O)(OH_2)(Pytacn)]^{2+}$ are formed when 3 equiv of CAN are added to a water solution of complex **1**. These species have long half-lives (>90 min), and no oxygen evolution was observed during their decay.[12,15] These experimental observations suggest that while these species are intermediates in the WO mechanism, by themselves they cannot produce O_2. Instead, experimentally it is found that $[Fe^{IV}(O)(OH_2)(Pytacn)]^{2+}$ needs to react with an excess of Ce^{IV} (2−3 equiv) for O_2 to be detected. However, it is possible to define a hypothetical scenario where the O—O bond is formed (see Scheme 1) but instead of O_2 release the formation of H_2O_2 is produced. For instance, the nucleophilic attack of a water molecule to $[Fe^{IV}(O)(OH_2)(Pytacn)]^{2+}$ would produce the formation of the O—O bond and the $Fe^{II}OOH$ intermediate (Scheme 1). Finally, the oxidation of $Fe^{II}OOH$ could produce O_2 and regenerate the resting state $[Fe^{IV}(O)$-$(OH_2)(Pytacn)]^{2+}$ (Scheme 2) or their protonation could produce H_2O_2. Indeed, this process could to some extent be operative. In this regard, we present herein DFT calculation

Table 1. Spin States Relative Free Energies (kcal·mol⁻¹) of the Fe^{IV} Intermediates for Complex 1 in the Two *cis*-Tautomers a and b

	1a-(O)(OH₂)	1b-(O)(OH₂)	1-(OH)(OH)
$S = 0$	10.8 (35.9)	10.0 (29.5)	21.8
$S = 1$	0.9 (2.2)	0.2 (2.4)	0.2
$S = 2$	0.0[a] (0.0)[b]	2.9 (4.9)	3.5

	1a-(O)(OH)	1b-(O)(OH)
$S = 0$	30.5 (22.1)	29.5 (28.5)
$S = 1$	3.1 (2.0)	1.3 (0.6)
$S = 2$	0.0[a] (0.0)[b]	1.5 (3.2)

[a]Free energies with respect to the most stable structure. [b]In parentheses, the free energy differences taking into account one solvent explicit water molecule.

Table 2. Selected Mulliken Spin Densities and Bond Distances for the Stationary Points Obtained in the Formation of the O–O Bond by an External Water Nucleophilic Attack to the $S = 2$ [Fe^{IV}(O)(OH₂)(Pytacn)]^{2+} Complex

	Ia$_{qt}$-(O)(OH₂)	TSa$_{qt}$-(O)(OH₂)	IIa$_{qt}$-(O)(OH₂)
$\rho(Fe)$	3.31	3.38	3.82
$\rho(O_a)$	0.47	0.15	0.04
$\rho(O_b)$	0.00	0.36	0.00
d(Fe-O$_a$)[b]	1.640	1.833	2.018
d(O$_a$-O$_b$)[b]	3.232	1.753	1.495
d(O$_b$-H$_c$)[b]	0.998	1.555	1.619

[a]L₁ stands for the Pytacn ligand. [b]Bond lengths are given in angstroms.

studies to provide an estimation of the energy barrier for the O–O bond formation reaction, and to address the viability of the process.

Water nucleophilic attack (WNA) over the terminal oxo of [Fe^{IV}(O)(OH₂)(Pytacn)]^{2+} results in formation of the O–O bond, forming a [Fe^{II}(OOH)(OH₂)(Pytacn)]^+ species and releasing a proton. Attempts to model the mechanism including only two water molecules failed. This is due to the poor description of the strong hydrogen bonds between the formed hydronium ion and the solvent water molecules given by the polarizable continuum model. Therefore, the two water molecules that form the first solvation shell of the hydronium ion have to be included as explicit water molecules to reproduce accurately such key hydrogen bonds during the O–O bond formation event. In the same line, we highlight that

previous theoretical studies[31−35] in related systems have shown that the consideration of the explicit water molecules forming the first solvation shell has a large influence on the energy of the O–O bond formation event.

Before exploring the O–O bond formation mechanism, we examined the relative energies of all different spin states for the iron IV species in the two possible *cis*-tautomers **a** and **b**. We also studied the influence of one solvent explicit water molecule in the spin splitting, to properly characterize the ground state and the most stable geometry for each Fe^{IV} species (see Table 1). The optimization of [Fe^{IV}(O)(OH₂)(Pytacn)]^{2+} with four explicit water molecules yields **Ia-(O)(OH₂)** in the $S = 2$ ground state, with Fe–O$_a$ and O$_a$-O$_b$ bond lengths of 1.640 and 3.232 Å, respectively (Table 2).[36] The difference between $S = 2$ and $S = 1$ states is only $\Delta G = 0.2$ kcal·mol⁻¹, which falls into
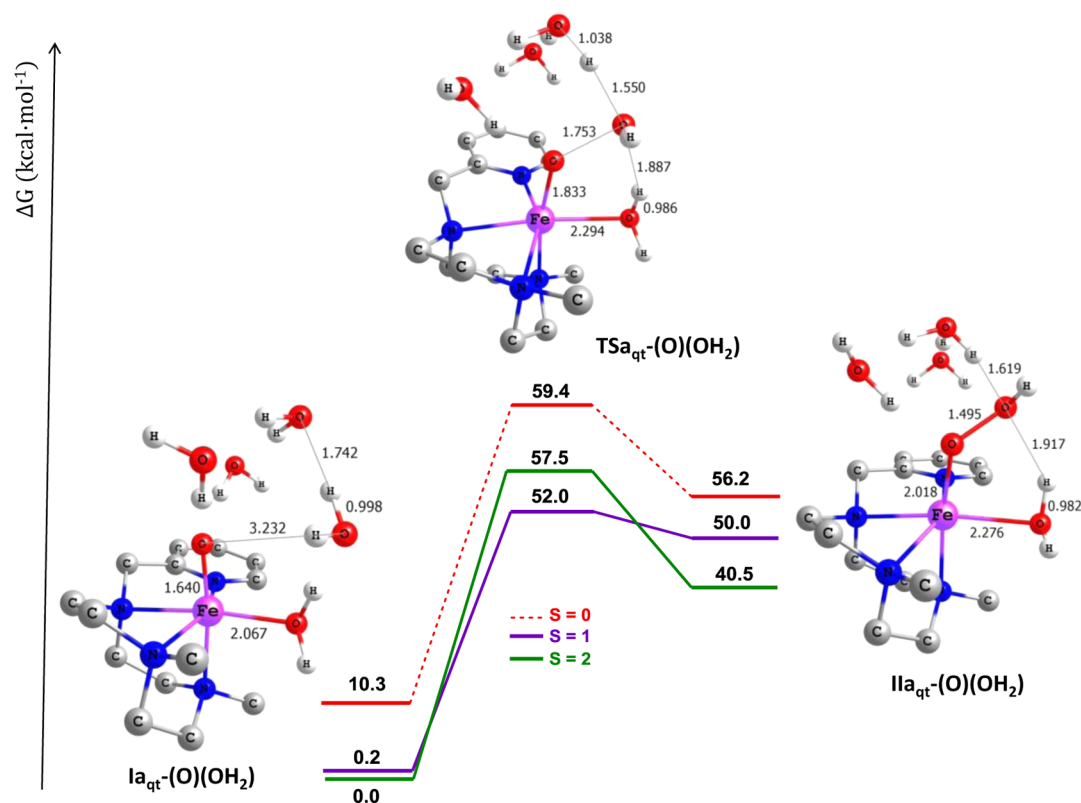
Figure 2. O−O bond formation profiles found for the **a** tautomer of $[Fe^{IV}(O)(OH_2)(Pytacn)]^{2+}\cdot 4H_2O$ for the $S = 0$, 1, and 2 spin states. Gibbs energy values are given in kcal·mol^{-1}. Figures inserted correspond to the $S = 2$ spin state, where selected bond distances (Å) are presented.

the mean error of the used DFT methodology. On the other hand, the $S = 0$ state is 10.3 kcal·mol^{-1} higher in energy than the spin state $S = 2$, and it is clearly not significant in the energy reaction path. Consequently, the $S = 1$ spin state should be carefully considered for the evaluation of the barrier of O−O bond formation. The most stable structure for the tautomer **1b**-**(O)(OH$_2$)**, which has a $S = 1$, is 2.4 kcal·mol^{-1} higher in energy than the ground state $S = 2$ **1a-(O)(OH$_2$)** (see Table 1). The free energy profile calculated for the O−O bond formation mechanism starting from **Ia-(O)(OH$_2$)** is summarized in Figure 2.

As Figure 2 shows, the O−O bond formation steps from $[Fe^{IV}(O)(OH_2)(Pytacn)]^{2+}\cdot 4H_2O$ (**Ia-(O)(OH$_2$)**) to yield $[Fe^{II}(OOH)(OH_2)(Pytacn)]^{+}\cdot H_3O^{+}(H_2O)_2$ (**IIa-(O)(OH$_2$)**) are connected through a concerted transition state (**TSa−OH$_2$**) for all studied spin states. The transition state lowest in energy was found to be the $S = 1$ **TSa$_t$-(O)(OH$_2$)**, which lies at 52.0 kcal·mol^{-1} over $S = 2$ $[Fe^{IV}(O)(OH_2)(Pytacn)]^{2+}\cdot 4H_2O$ (see Supporting Information, Figure SI.1 for the geometries in the $S = 0$ and $S = 1$ spin states). However, after a spin crossing, the reaction evolves to the spin state most stable $S = 2$ Fe^{II} hydroperoxo product, **IIa$_{qt}$-(O)(OH$_2$)**, which was found 9.5 and 15.7 kcal·mol^{-1} lower in energy than the $S = 1$ and $S = 0$ products, respectively (see Figure 2). Taking these results into consideration, the O−O bond formation pathway is not feasible through $[Fe^{IV}(O)(OH_2)(Pytacn)]^{2+}$. This result is indeed in complete agreement with the experimental observation that $[Fe^{IV}(O)(OH_2)(Pytacn)]^{2+}$ in water does not evolve to produce molecular oxygen. Nevertheless, we noted that the inverse reaction $S = 2$ path from Fe^{II} to Fe^{IV} species presents a very low energy barrier of 17.0 kcal·mol^{-1}, suggesting that the non-heme Fe^{IV}=O species could be generated by direct

reaction of Fe^{II} and H$_2$O$_2$ in water. This reaction actually finds precedent in some bioinspired synthetic complexes with related nitrogen based ligands,[37] and it is also reminiscent of the O−O breakage mechanism operating in non-heme dependent oxygenases.[38]

O−O Bond Formation Mechanism through [Fe^{IV}(O)-(OH)(Pytacn)]$^{+}$. The B3LYP-D$_2$ pK_a value of 10 of the water ligand in $[Fe^{IV}(O)(OH_2)(Pytacn)]^{2+}$ indicates that the oxo-aqua complex is the stable species under catalytic conditions (pH = 1). To obtain a consistent pK_a value, we have studied the effect of increasing the number of explicit solvent water molecules, obtaining a pK_a convergence value close to 10 (see Supporting Information, Table SI.1). At the catalytic pH value of 1, the Gibbs energy of $[Fe^{IV}(O)(OH)(Pytacn)]^{+}$ is 12.0 kcal·mol^{-1} higher than $[Fe^{IV}(O)(OH_2)(Pytacn)]^{2+}$. This result implies that the formation of a O−O bond through intermediate $[Fe^{IV}(O)(OH)(Pytacn)]^{+}$ is very unlikely. Nevertheless, $[Fe^{IV}(O)(OH)(Pytacn)]^{+}$ presents a OH ligand *cis* to the oxo group that could aid the O−O bond formation by acting as an internal Brønsted base accepting a proton from the water molecule. To evaluate the kinetic viability of the processes, two possible O−O bond formation mechanisms were explored: an internal base assisted mechanism, where the OH ligand acts as a proton acceptor,[16,39] and an external base assisted mechanism, where a water solvent molecule acts as an external base (Figure 3).

Internal Base Assisted Mechanism. In this case, only a single water molecule is required to be explicitly modeled. The most stable structure for $[Fe^{IV}(O)(OH)(Pytacn)]^{+}\cdot H_2O$ was found among the $S = 2$ spin-state structures (**Ia$_{qt}$-(O)(OH$_{int}$)**). Structures with spin states $S = 1$ and $S = 0$ are 2.0 kcal·mol^{-1} and 22.1 kcal·mol^{-1} higher in energy than the ground state (see
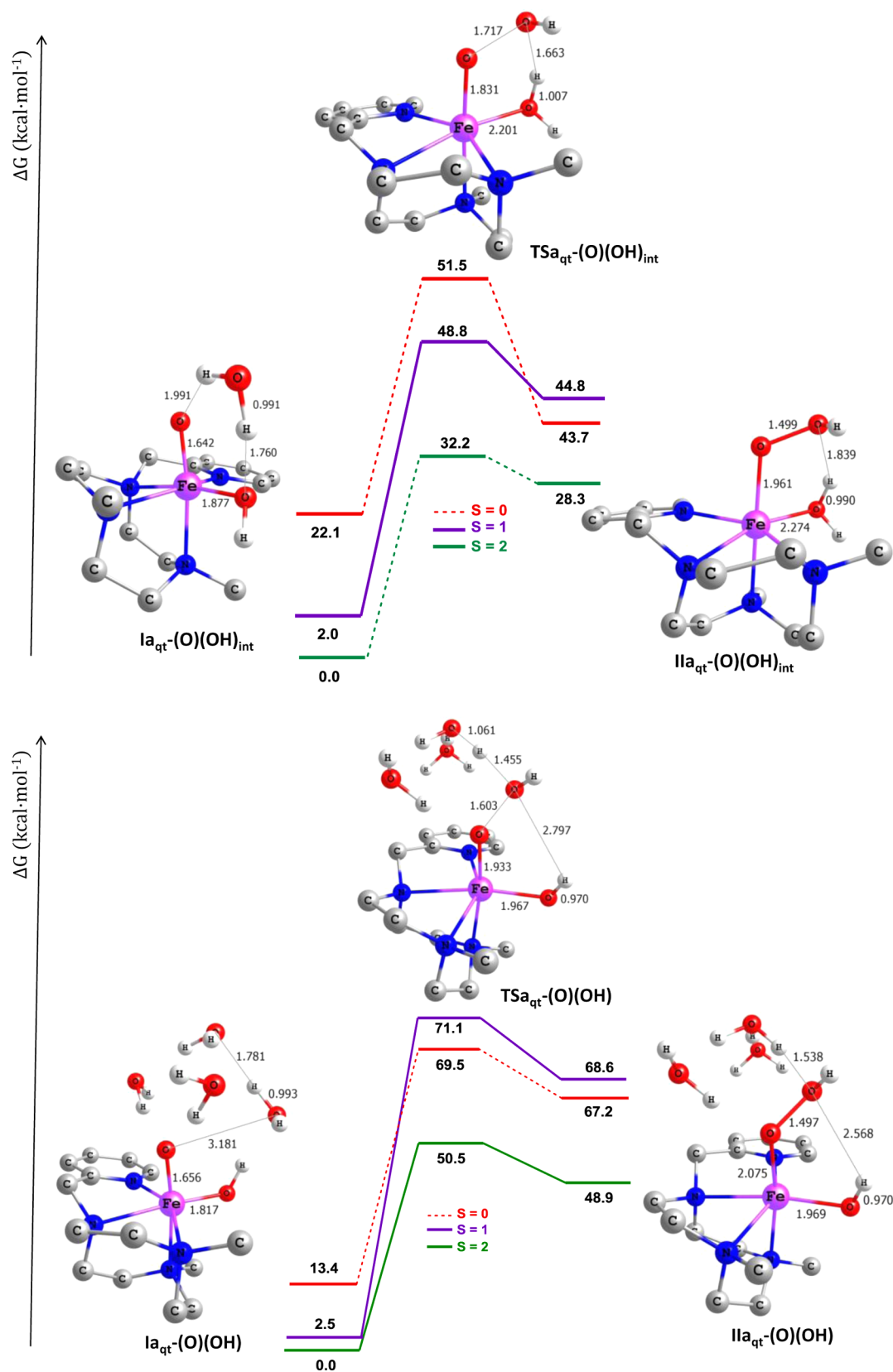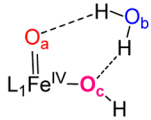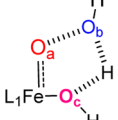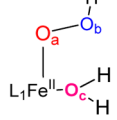
Figure 3. Internal (top) and external (bottom) base assisted O–O bond formation mechanisms from the tautomer **a** $[Fe^{IV}(O)(OH)(Pytacn)]^+$ intermediate. Gibbs energy values are given in kcal·mol^{-1}. Selected bond distances in Å are indicated in the figures corresponding to the stationary points of the $S = 2$ reaction profile.
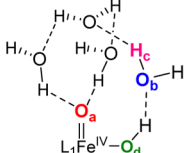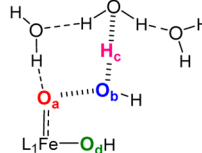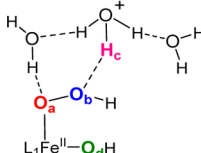
Supporting Information, Figure SI.2). In the water adduct $[Fe^{IV}(O)(OH)(Pytacn)]^+ \cdot H_2O$, the formation of two hydrogen

bonds between the water molecule and the oxo and hydroxo ligands of $[Fe^{IV}(O)(OH)(Pytacn)]^+$ yields the most stable

Table 3. Selected Mulliken Spin Densities and Bond Distances for the $S = 2$ Stationary Points Involved in the O−O Bond Formation Mechanism from $[Fe^{IV}(O)(OH)(Pytacn)]^+$ Species

	Ia_{qt}-(O)(OH)$_{int}$	TSa_{qt}-(O)(OH)$_{int}$	IIa_{qt}-(O)(OH)$_{int}$
$\rho(Fe)$	3.25	3.91	3.81
$\rho(O_a)$	0.44	0.08	0.06
$\rho(O_b)$	0.00	-0.21	0.00
$\rho(O_c)$	0.12	0.03	0.02
$d(Fe-O_a)^b$	1.642	1.831	1.961
$d(O_a-O_b)^b$	2.803	1.717	1.499

|	Ia_{qt}-(O)(OH)	TSa_{qt}-(O)(OH)	IIa_{qt}-(O)(OH)
$\rho(Fe)$	3.29	3.84	3.80
$\rho(O_a)$	0.36	0.02	0.03
$\rho(O_b)$	0.00	-0.09	-0.01
$\rho(O_d)$	0.14	0.10	0.09
$d(Fe-O_a)^b$	1.656	1.933	2.075
$d(O_a-O_b)^b$	3.181	1.603	1.497
$d(Fe-O_d)^b$	1.817	1.967	1.968
$d(O_b-H_c)^b$	0.993	1.455	1.538

^{a}L$_1$ stands for the Pytacn ligand. ^{b}Bond lengths are given in angstroms.

structure. From this intermediate, the reaction proceeds via nucleophilic attack of the O atom of the water molecule to the oxo group to form the transition state TSa_{qt}-(O)(OH)$_{int}$ ($\Delta G^{\ddagger}$ = 32.2 kcal·mol^{-1}). At this stage, a proton is transferred from the water molecule to the OH ligand with concomitant O−O bond formation. The reorganization enlarges the Fe-oxo bond to 0.189 Å and shortens the O−O bond distance to 1.086 Å. Mulliken population analysis of the TSa_{qt}-(O)(OH)$_{int}$ showed a spin density value of −0.21 at the oxygen atom of the water molecule, a spin density decrease of 0.36 at the oxo ligand, and an increase of 0.66 at the iron center (Table 3). These spin density reorganizations suggest a partial electron transfer from the water molecule to the iron-oxo moiety along the reaction coordinate, responsible for the reduction of the iron oxidation state. The concerted transition state leads to the formation of the Fe^{II} hydroperoxo product (IIa_{qt}-(O)(OH$_{int}$)) with a O−O bond length of 1.499 Å. The process is endergonic, with a ΔG value of 28.3 kcal·mol^{-1}. Indeed, the $\Delta G^{\ddagger}$ of the O−O bond formation through $[Fe^{IV}(O)(OH)(Pytacn)]^+$·H$_2$O increases to 40.3 kcal·mol^{-1} if the most stable $[Fe^{IV}(O)(OH_2)(Pytacn)]^{2+}$ species is considered as the reactant.

To this point, we have only considered the O−O bond formation mechanism performed by tautomer **a** of $[Fe^{IV}(O)-$(OH)(Pytacn)]$^+$. The free energy difference between the ground spin states of the two tautomers of the $[Fe^{IV}(O)-$(OH)(Pytacn)]$^+$·H$_2$O intermediate indicates that Ia_{qt}-(O)-(OH)$_{int}$ is slightly more stable than the Ib_t-(O)(OH)$_{int}$ species
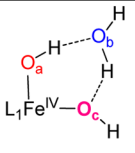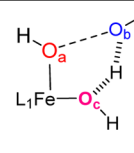
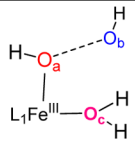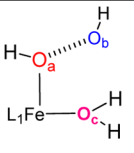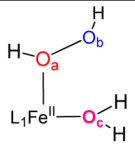($\Delta G^{\ddagger}$ = 0.6 kcal·mol^{-1}). Therefore, to analyze the kinetic feasibility of the process, it is important to evaluate also the same event conducted by tautomer **b**. The spin-state energy profiles for tautomer **b** show the same reactivity trend already described for **a**, with an O−O bond formation energy barrier slightly higher of $\Delta G^{\ddagger}$ = 32.8 kcal·mol^{-1} (see Supporting Information, Figure SI.3). In summary, from the kinetic point of view, the barrier of this reaction is too high to occur at room temperature, and from the thermodynamic point of view, the reaction is clearly disfavored due to its strong endergonic character.

External Base Assisted Mechanism. This mechanism requires the inclusion of at least four explicit water molecules to correctly reproduce the stabilization of the formed hydronium ion by means of hydrogen bonds. In the same line, a large influence with respect to the number of explicit water molecules composing the first solvation shell on the O−O bond formation event has been also found in previous theoretical studies.[31−35] The $[Fe^{IV}(O)(OH)(Pytacn)]^+$·4H$_2$O external base assisted O−O bond formation by the tautomeric form **a** also occurs through a $S = 2$ concerted transition state (TSa_{qt}-(O)(OH), $\Delta G^{\ddagger}$ = 50.5 kcal·mol^{-1}), 19.0 and 20.6 kcal·mol^{-1} lower in Gibbs energy than the $S = 0$ and $S = 1$ transition states, respectively (see Figures 3 and Supporting Information, Figure SI.4). The high Gibbs energy barrier and the Gibbs energy reaction (48.9 kcal·mol^{-1}) obtained for the IIa_{qt}-
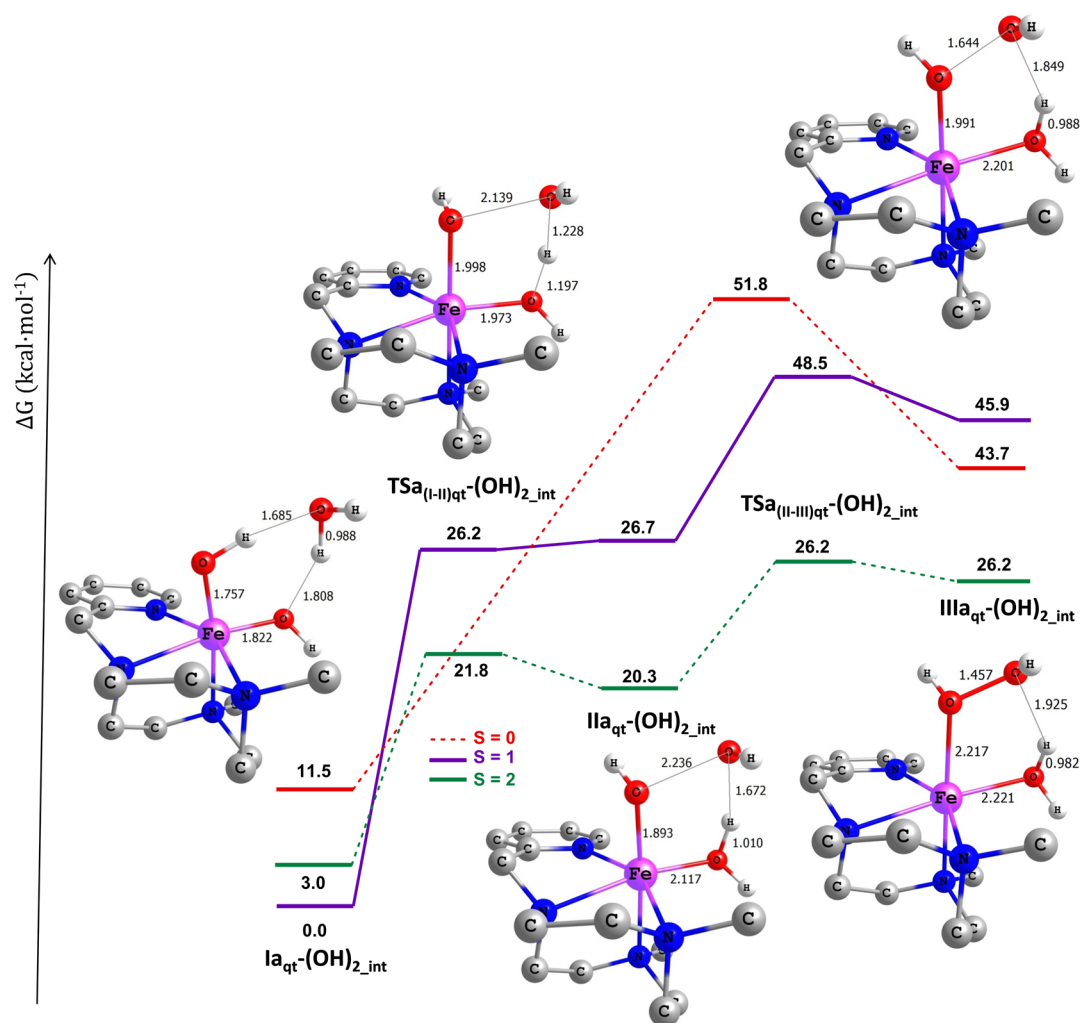
Figure 4. Internal base assisted O−O bond formation mechanisms from the tautomer **a** of $[Fe^{IV}(OH)(OH)(Pytacn)]^{2+}$ intermediate. Gibbs energy values are given in kcal·mol^{-1}. Selected bond distances (Å) of stationary points on the $S = 2$ reaction profile are indicated in the figures.

Table 4. Selected Mulliken Spin Densities and Bond Distances for the Stationary Points Obtained in the Formation of the O−O Bond by External Water Nucleophilic Attack to the $S = 2$ $[Fe^{IV}(OH)(OH)(Pytacn)]^{2+}$ Complex

	$Ia_{qt}\text{-}(OH)_{2\_int}$	$TSa_{(I\text{-}II)qt}\text{-}(OH)_{2\_int}$	$IIa_{qt}\text{-}(OH)_{2\_int}$	$TSa_{(II\text{-}III)qt}\text{-}(OH)_{2\_int}$	$IIIa_{qt}\text{-}(OH)_{2\_int}$
$\rho(Fe)$	3.49	4.29	4.30	3.97	3.82
$\rho(O_a)$	0.13	-0.34	-0.05	0.00	0.01
$\rho(O_b)$	0.01	-0.56	-0.79	-0.23	0.00
$\rho(O_c)$	0.18	0.13	0.07	0.03	0.02
$d(Fe\text{-}O_a)^b$	1.76	2.00	1.89	1.99	2.22
$d(O_a\text{-}O_b)^b$	2.67	2.14	2.12	1.64	1.46

^{a}L$_1$ stands for the Pytacn ligand. ^{b}Bond lengths are given in angstroms.

(O)(OH) indicates that O−O bond formation is kinetically and thermodynamically unviable through this mechanism.

Unexpectedly, the energy barrier found for the external attack of the water molecule to the oxo group on $[Fe^{IV}(O)\text{-}(OH_2)(Pytacn)]^{2+}\cdot 4H_2O$ is slightly higher than that for $[Fe^{IV}(O)(OH)(Pytacn)]^+\cdot 4H_2O$, despite that the former is

expected to be more electrophilic, owing to charge considerations. This phenomenon could have its origin in the hydrogen bond formed between the nucleophilic water molecule and the *cis* ligand to the oxo group. The O(nucleophilic water)−H(*cis* ligand) hydrogen bond is stronger in $Ia_{qt}\text{-}(O)(OH_2)$ ($d_{(Ob\text{-}H)} = 1.576$ Å) than in $Ia_{qt}\text{-}$

Table 5. Free Energy Differences (ΔG) and pK_a Values for the Proton Dissociation of HNO$_3$ Assisted by Several Water Clusters

	ΔG (kcal·mol^{-1})	pK_a[a]
HNO$_3$	125.7 (270)[b]	93.5 (199.4)[c]
HNO$_3$ + H$_2$O	10.0	7.4
HNO$_3$ + 2H$_2$O	2.1	1.5
HNO$_3$ + 3H$_2$O	−1.9	−1.4
exp	−1.9	−1.4

[a]The pK_a values are evaluated at room temperature and atmospheric pressure. [b]In parentheses are shown the electronic energy difference obtained from ref 17 and the corresponding pK_a value. [c]Experimental pK_a obtained from ref 41.

(O)(OH) ($d_{(Ob-H)}$ = 1.761 Å), producing a less nucleophilic water molecule and then a higher energy barrier when a *cis*-aqua ligand is present.

On the other hand and more remarkably, when the *cis*-OH ligand acts as an internal base, the O−O bond formation barrier is reduced in large extent with respect to the external mechanism ($\Delta\Delta G^{\ddagger}$ = 18.3 kcal·mol^{-1}, Figure 3). Even taking into account the free energy required for the deprotonation equilibrium of [Fe^{IV}(O)(OH$_2$)(Pytacn)]$^{2+}$ under catalytic conditions (12.0 kcal·mol^{-1}), the O−O bond formation barrier for the internal mechanism remains lower in energy by $\Delta\Delta G^{\ddagger}$ = 6.3 kcal·mol^{-1}. This result has implications in the future ligand design for the development of iron catalyst for the water oxidation reaction, as the introduction of internal bases clearly reduces the energy of the barrier. But in this case, the energy reduction of the barrier is not enough to allow the reaction of [Fe^{IV}(O)(OH)(Pytacn)]$^+$ with water to occur at room temperature. Finally, an analysis of the magnitude of the enthalpic and entropic contributions to the O−O bond formation free energy barrier was performed at the B3LYP/6-31G*/SMD level to elucidate the origin of the internal base effect. For the internal mechanism, the enthalpy and entropy of activation are 37.2 kcal·mol^{-1} and 2.9 cal·mol^{-1}·K^{-1} respectively, while, for the external mechanism, they are $\Delta H^{\ddagger}$ = 56.8 kcal·mol^{-1} and $\Delta S^{\ddagger}$ = 0.6 cal·mol^{-1}·K^{-1}. Indeed, this event is mainly controlled by the enthalpic term. Therefore, it can be rationalized by the preference of the final Fe^{II}−OOH·4H$_2$O product to act as a Brønsted base (pK_a = 16.0), locating the positive charge present on the ejected proton at the complex instead to delocalize it to the bulk water solvent.

O−O Bond Formation Mechanism through [Fe^{IV}(OH)(OH)(Pytacn)]$^{2+}$. Finally, the last Fe^{IV} complex to consider is the bis-hydroxo [Fe^{IV}(OH)(OH)(Pytacn)]$^{2+}$, which is a structural isomer of [Fe^{IV}(O)(OH$_2$)(Pytacn)]$^{2+}$. Indeed, [Fe^{IV}(OH)(OH)(Pytacn)]$^{2+}$ is 2.1 kcal·mol^{-1} higher in free energy than the Fe^{IV}-aqua complex (one explicit water molecule interacting with the oxygen moieties of the complexes was considered in the models). Therefore, the O−O bond formation mechanism through the Fe^{IV}-bishydroxo complex has also been investigated (Figure 4). In this case, only one explicit water molecule is enough to ensure a correct description of the internal base assisted mechanism. We have explored the mechanism for both possible tautomers **a** and **b**, which are virtually isoenergetic (0.5 kcal·mol^{-1}). We first explored the O−O bond formation event with the tautomer **a**, allowing proper comparison with the previous mechanisms. The [Fe^{IV}(OH)(OH)(Pytacn)]$^{2+}$·H$_2$O complex presents a S = 1 ground spin state (**Ia$_t$-(OH)$_{2\_int}$**). The S = 2 and S = 0 spin

states lie 3.0 kcal·mol^{-1} and 11.5 kcal·mol^{-1} higher in free energy than the triplet ground state, respectively (see Supporting Information, Figure SI.5). The starting **Ia$_t$-(OH)$_{2\_int}$** includes the interaction of the two hydroxo ligands with one hydrogen and the oxygen atom of the water molecule through two hydrogen bonds (Figure 4). In contrast with the previous discussed mechanism, the proton transfer and the O−O bond formation do not occur simultaneously. Instead, we have observed a two-step mechanism. All attempts to obtain the concerted mechanism failed. The first step involves the rotation of one O$_a$H group of **Ia$_t$-(OH)$_{2\_int}$** to allow the interaction between O$_a$ and the O$_b$ of the water molecule, and the proton transfer from the nucleophilic water molecule to the O$_c$H group (**TSa$_{(I-II)qt}$-(OH)$_{2\_int}$**: $\Delta G^{\ddagger}$ = 21.8 kcal·mol^{-1}). This yields the intermediate **IIa$_{qt}$-(OH)$_{2\_int}$** (ΔG = 20.3 kcal·mol^{-1}) (Table 4 and Figure 4). In **IIa$_{qt}$-(OH)$_{2\_int}$**, the proton is completely transferred, forming a second water molecule. The spin densities on the iron center of **IIa$_{qt}$-(OH)$_{2\_int}$** (ρ(Fe) = 4.30) and on the oxygen atom of the former nucleophilic water molecule (ρ(O$_b$) = −0.79) reveal an antiferromagnetically coupling between O$_b$H and {Fe(OH)(OH$_2$)} fragments. This suggests an electron transfer between the two previous groups leading to a formal Fe^{III} center. The difference in mechanism found among isomers could be rationalized with the electrophilicity of the iron complex. For instance, the difference in energy between [Fe^{IV}(OH)(OH)(Pytacn)]$^{2+}$ and [Fe^{IV}(O)(OH$_2$)(Pytacn)]$^{2+}$ isomers is translated into a reduction potential difference of 100 mV. Therefore, [Fe^{IV}(OH)(OH)(Pytacn)]$^{2+}$ is relatively more oxidant than [Fe^{IV}(O)(OH$_2$)(Pytacn)]$^{2+}$, which could explain the preference for a direct hydrogen transference transfer before the O−O bond formation step. This is consistent with the O−O bond formation mechanism found for Fe^{V}(O)(OH) species.[15,16]

Finally, in the second step, **IIa$_{qt}$-(O)(OH)$_{2\_int}$** connects with the **IIIa$_{qt}$-(O)(OH)$_{2\_int}$** Fe^{II} complex via the transition state **TSa$_{(II-III)qt}$-(O)(OH)$_{2\_int}$**, which is the TOF determining transition state (TDTS) ($\Delta G^{\ddagger}$ = 26.2 kcal·mol^{-1}), forming the O−O bond. Considering the lowest Fe^{IV}-oxo isomer ([Fe^{IV}(O)(OH$_2$)(Pytacn)]$^{2+}$) as the starting point of the reaction, the barrier increases up to 28.3 kcal·mol^{-1}. Thus, this mechanism is kinetically unviable. The reaction evolves through the S = 2 potential energy surface. For the S = 0 energy surface, only the concerted transition state (**TSa$_s$-(OH)$_{2\_int}$**: $\Delta G^{\ddagger}$ = 51.8 kcal·mol^{-1}, Supporting Information, Figure SI.5) has been located, which is too high in energy to be directly involved in the O−O bond formation event. Finally, the **b** tautomer of [Fe^{IV}(OH)(OH)(Pytacn)]$^{2+}$ presents a very similar free energy profile with a free energy barrier for the O−O bond formation step of 33.3 kcal·mol^{-1} (see Supporting Information, Figure SI.6), which again is too high to occur at room temperature.

Comparison with the Catalytic Cycle Proposed by Kasapbasi et al. While our computations are quite conclusive in showing that the iron(IV)-oxo species [Fe^{IV}(O)(OH)(Pytacn)]$^+$, [Fe^{IV}(O)(OH$_2$)(Pytacn)]$^{2+}$, and [Fe^{IV}(OH)(OH)(Pytacn)]$^{2+}$ cannot form the O−O bond and oxidize the water molecule, a recent report by Kasapbasi et al. indicated otherwise (Figure 1b). A close analysis of this work shows that the thermodynamic driving force of the catalytic cycle depends on the energy gain of the protonation of nitrate anions. The authors proposed that a nitrate anion present at the coordination sphere of the reduced CAN acts as a Brønsted base to form the [Fe^{IV}(O)(OH)(Pytacn)]$^+$ complex. This

5482

dx.doi.org/10.1021/ic500108g | *Inorg. Chem.* 2014, 53, 5474−5485

species performs the O−O bond formation event, through the nucleophilic attack of a solvent water molecule to the Fe^{IV}=O moiety. The protonation of the formed hydroperoxo ligand leads to the release of hydrogen peroxide, which is oxidized to molecular oxygen by Ce^{IV} and generates an open vacant site on the iron center. In the next step, the water molecule occupies the free vacant site to form a $[Fe^{IV}(OH_2)_2(Pytacn)]^{4+}$ intermediate. Finally, the nitrate ions abstract two protons of the Fe^{IV} aqua complex to recover the resting-state species.
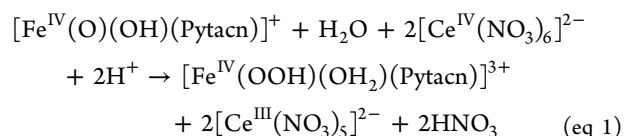
From a methodological point of view, one of the main differences between the present work and that of Kasapbasi et al. is how the solvent effect has been computed. In the latter case, the conductor polarizable continuum model (CPCM) was employed,[40] without consideration of any explicit water molecule. However, this methodology cannot describe accurately the hydrogen bonds and dispersion effects present in the water media. The hydrogen bonding needs to be considered, especially when protic solvents are involved directly in the reaction and the studied mechanistic step releases or captures protons.[34,35] Furthermore, the enthalpy and entropy corrections, which may be decisive to ensure an accurate description of the thermodynamics and kinetics of the WO reaction, were not included in Kasapbasi calculations. To clarify these points, we have examined and found that the DFT reaction free energy of the nitrate protonation depends strongly on the number of explicit water molecules included in the proton first solvation shell. The influence of the number of explicit water molecules of the proton first solvation shell on the acidic character of the HNO_3 in the aqueous phase is summarized in Table 5 (see Supporting Information, Figure SI.7 for the proton hydrated cluster geometries).

The pK_a of the gas-phase deprotonation process is very far from the experimental value due to the description of the proton as a free ion. This large deviation is even true if solvent effects are included only through an implicit solvation model, showing the weakness of the SMD model for this case of study. Addition of neither enthalpy nor entropy corrections allows reproducing the experimental observed behavior. The results clearly improve the inclusion of one explicit water molecule, but still unreliable pK_a values (7.4) were obtained. A more accurate pK_a result (1.5) was obtained by the inclusion of two water molecules, already reproducing the strong acidic behavior of the nitric acid. But with three explicit water molecules the experimental HNO_3 pK_a value is nicely reproduced. Furthermore, for HNO_3 the pK_a values show a clear rapid convergence with respect to the number of explicit water molecules included in the proton solvation shell.
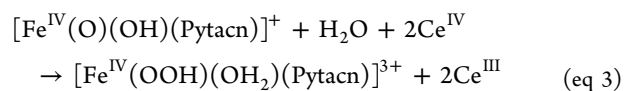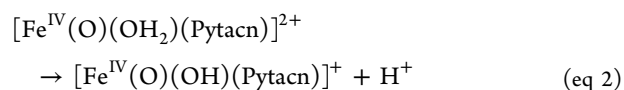
Consideration of the enthalpy and entropic corrections and three explicit water molecules into the calculations makes nitrate ions poor hydrogen atom acceptors, as may actually be expected considering the low experimental pK_a of HNO_3 (−1.4). It must be emphasized that the origin of the acid/base character of nitrate species specifically falls in the correct description of the solvated free protons in the bulk water solvent, not in the solvation effects on the NO_3 itself. The microsolvation on the whole system (nitrate + proton) was also explored, leading to its expected acid character when the number of explicit molecules increases (See Supporting Information, Table SI.2 and Figures SI.8−9). The consequence of the inclusion of explicit water molecules in the calculations is that the driving force for the water oxidation reaction proposed by Kasapbasi and co-workers, i.e. the protonation of nitrate anions, is removed. Then, the reaction of $[Fe^{IV}(O)(OH)-$

$(Pytacn)]^+$ and $[Fe^{IV}(O)(OH_2)(Pytacn)]^{2+}$ with water becomes computationally unfeasible under ambient experimental conditions.

Although the present study discards the WNA mechanism on a Fe^{IV}=O moiety, we cannot ignore the possible involvement of CAN species in the O−O bond formation event. Kasapbasi et al. proposed that $[Ce^{IV}(NO_3)_6]^{2-}$ could accept the two electrons transferred during the WNA on the oxo moiety of $[Fe^{IV}(O)(OH)(Pytacn)]^+$, allowing the formation of a $[Fe^{IV}(OOH)(OH_2)(Pytacn)]^{3+}$ intermediate (eq 1). Thus, to corroborate the viability of this process, we evaluated the free energy of this reaction at our more accurate level of calculation, obtaining indeed the exergonic character observed by Kasapbasi et al. ($\Delta G = -283.0$ kcal·mol^{-1}). However, as explained above, the free energy of solvation for a free proton is not correctly described in the SMD model, and the experimental value must be used, which strongly decreases the exergonic character of the reaction ($\Delta G = -23.1$ kcal·mol^{-1}). Nevertheless, from a thermodynamic point of view, this reaction is feasible at room temperature.

$$[Fe^{IV}(O)(OH)(Pytacn)]^+ + H_2O + 2[Ce^{IV}(NO_3)_6]^{2-}$$
$$+ 2H^+ \rightarrow [Fe^{IV}(OOH)(OH_2)(Pytacn)]^{3+}$$
$$+ 2[Ce^{III}(NO_3)_5]^{2-} + 2HNO_3 \qquad (eq\ 1)$$

But the nature of Ce nitrate species in aqueous solution is not well-known, and then the free energy change obtained from the DFT calculation of $[Ce^{IV}(NO_3)_6]^{2-}$ and $[Ce^{III}(NO_3)_5]^{2-}$ may not be reliable. A more realistic energy balance can be obtained by taking into account the free energy obtained from the experimental Ce(IV) reduction potential ($E^\circ = 1.61$ V vs SHE at pH = 1), giving a slightly endergonic but still feasible process when the deprotonation step is considered (eqs 2 and 3, $\Delta G = 3.4$ kcal·mol^{-1}). However, as we have previously shown, the O−O bond formation catalyzed by $[Fe^{IV}(O)(OH)-(Pytacn)]^+$, is kinetically not allowed at catalytic conditions.

$$[Fe^{IV}(O)(OH_2)(Pytacn)]^{2+}$$
$$\rightarrow [Fe^{IV}(O)(OH)(Pytacn)]^+ + H^+ \qquad (eq\ 2)$$

$$[Fe^{IV}(O)(OH)(Pytacn)]^+ + H_2O + 2Ce^{IV}$$
$$\rightarrow [Fe^{IV}(OOH)(OH_2)(Pytacn)]^{3+} + 2Ce^{III} \qquad (eq\ 3)$$

The theoretical data suggest a WO catalytic cycle where the oxidizing power of the Ce^{IV} is the driving force of the reaction. This sacrificial oxidant may allow the generation of highly electrophilic Fe^V=O species, which catalyzes the O−O bond formation event. This hypothesis was corroborated evaluating the energetic accessibility of the V oxidation state through the calculation of the PCET redox potential from $[Fe^{IV}(O)(OH_2)-(Pytacn)]^{2+}$ to $[Fe^V(O)(OH)(Pytacn)]^{2+}$ species. The $E^\circ(PCET)$ value at pH = 1 does not change significantly between tautomer **a** (1.69 V vs SHE) and **b** (1.74 V vs SHE), and falls into the interval of 1.6−1.7 V vs SHE associated with the reduction potential of Ce^{IV} under catalytic conditions.[16] Therefore, CAN presents enough oxidizing power to reach the $[Fe^V(O)(OH)(Pytacn)]^{2+}$ species. We had previously presented that $[Fe^V(O)(OH)(Pytacn)]^{2+}$ species have a viable energy barrier for the O−O bond formation of 18.5 kcal·mol^{-1}.[16] Finally, the oxidation potentials to reach the $[Fe^{VI}(O)(OH)(Pytacn)]^{3+}$ and $[Fe^{VI}(O)(O)(Pytacn)]^{2+}$ species were also calculated, obtaining values of $E^\circ = 3.11$ and 2.26

V, which are far from the oxidizing capacity of CAN (E° = 1.61 V at pH = 1). Altogether, the data presented clearly illustrate that the O−O bond formation likely could not directly occur by the {Fe^{IV}(Pytacn)} nor by {Fe^{VI}(Pytacn)} species. Thus, both experimental and DFT evidence point to [Fe^V(O)(OH)(Pytacn)]$^{2+}$ species as the most likely responsible for the O−O bond formation event under catalytic conditions.

CONCLUSIONS

Our computational results confirm the kinetic unviability of [Fe^{IV}(O)(OH)(Pytacn)]$^+$, [Fe^{IV}(O)(OH$_2$)(Pytacn)]$^{2+}$, and

Scheme 3. Summary of All the O−O Bond Formation Pathways Involving Fe^{IV}(O) and Fe^V(O) Species[a]
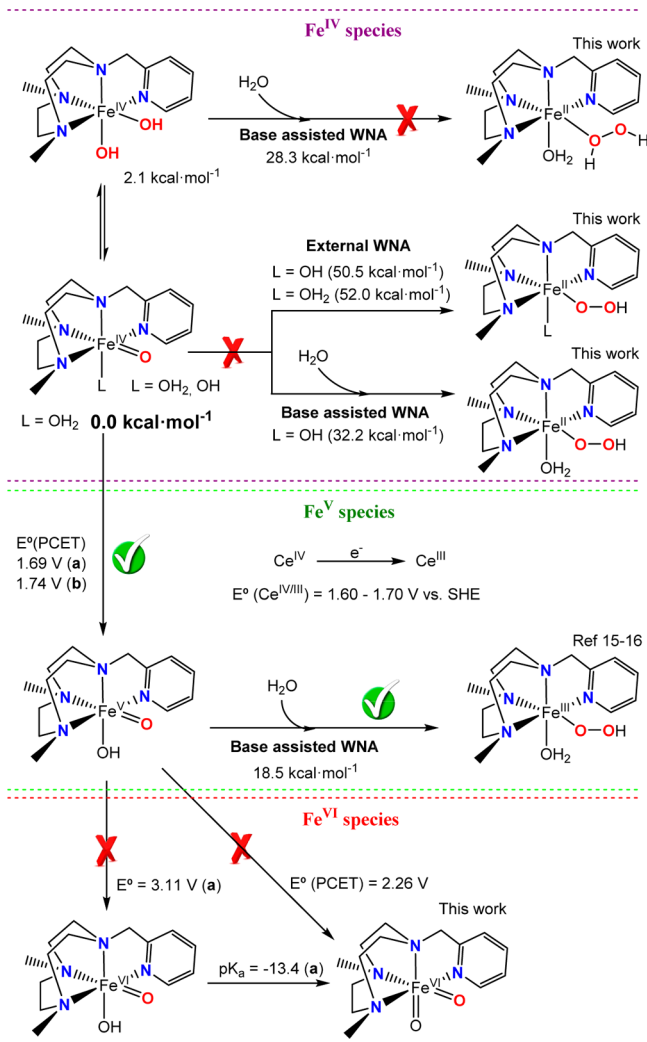
[a]The lowest energy barrier for the O−O bond formation starting from {Fe^{IV}} species is around 28 kcal·mol^{-1}. In addition, we also reported that the redox couple Fe$^{V/VI}$ is not accessible under catalytic conditions. The redox values are relative to the SHE electrode at pH = 1. The free energies of the TS are relative to the [Fe^{IV}(O)(OH$_2$)(Pytacn)]$^{2+}$ and [Fe^V(O)(OH)(Pytacn)]$^{2+}$, respectively. WNA stands for Water Nucleophilic Attack.

[Fe^{IV}(OH)(OH)(Pytacn)]$^{2+}$ species to perform the O−O bond formation event at room temperature, as well as the high endergonic nature of the intermediates formed after the O−O bond formation. These results are in complete agreement with

the experimentally observed inactivity of [Fe^{IV}(O)(OH$_2$)(Pytacn)]$^{2+}$ species in aqueous solution, and discarding the formation of H$_2$O$_2$. Thus, our results also discard the viability of WOC cycles based on the feasibility of Fe^{IV}(O) species to catalyze the formation of the O−O bonds. Our results also show that Fe^{VI} species are not accessible under catalytic conditions. On the contrary, our investigations have previously highlighted the need to access the high-oxidation-state [Fe^V(O)(OH)(Pytacn)]$^{2+}$ species[15,16] in order to yield the O−O bond formation, providing more confidence on the WOC mechanistic proposal involving Fe^V(O) as the active species (Scheme 3). Moreover, the results indicate that the introduction of an internal base in the coordination sphere of the iron complex reduces the energy of the O−O bond formation barrier. These results clearly have implications on the future design of iron based catalysts for WO.

This work also highlights the importance of the explicit treatment of the hydrogen bonding network between the solvent molecules and the protons to achieve a good correlation with experimental data. Although our results demonstrated that the proposed catalytic cycle of Kasapbasi et al. does not correctly describe the WO mechanism performed by iron complex **1** in the condensed phase, albeit it may be useful to gain insight about the gas-phase reactivity, such as the conditions found in mass spectrometry experiments.

ASSOCIATED CONTENT

Ⓢ Supporting Information

Selected bond distances (Å) of all the optimized structures, their corresponding Cartesian coordinates, and free energy data for iron and nitrate species. This material is available free of charge via the Internet at http://pubs.acs.org.

AUTHOR INFORMATION

Corresponding Authors
*E-mail (J.M.L.): josepm.luis@udg.edu.
*E-mail (J.L.-F.): julio.lloret@udg.edu.
Notes
The authors declare no competing financial interest.

ACKNOWLEDGMENTS

REFERENCES

(1) (a) Barber, J. *Philos. Trans. R. Soc., A* **2007**, *365*, 1007−1023. (b) Ferreira, K. N.; Iverson, T. M.; Maghlaoui, K.; Barber, J.; Iwata, S. *Science* **2004**, *303*, 1831−1838. (c) Umena, Y.; Kawakami, K.; Shen, J. R.; Kamiya, N. *Nature* **2011**, *473*, 55−65.

(2) (a) Yachandra, V. K.; Sauer, K.; Klein, M. P. *Chem. Rev.* **1996**, *96*, 2927−2950. (b) Messinger. *J. Phys. Chem. Chem. Phys.* **2004**, *6*, 4764−4771. (c) Cox, N.; Pantazis, D. A.; Neese, F.; Lubitz, W. *Acc. Chem. Res.* **2013**, *46*, 1588−1596. (d) Siegbahn, P. E. M. *Acc. Chem. Res.* **2009**, *42*, 1871−1880. (e) Isobe, H.; Shoji, M.; Yamanaka, S.; Umena, Y.; Kawakami, K.; Kamiya, N.; Shen, J. R.; Yamaguchi, K. *Dalton Trans.* **2012**, *41*, 13727−13740. (f) McEvoy, J. P.; Brudvig, G. W. *Chem. Rev.* **2006**, *106*, 4455−4483. (g) Sproviero, E. M.; Gascon, J. A.; McEvoy, J. P.; Brudvig, G. W.; Batista, V. S. *Coord. Chem. Rev.* **2008**, *252*, 395−415. (h) Pecoraro, V. L.; Baldwin, M. J.; Caudle, M. T.; Hsieh, W.-Y.; Law, N. A. *Pure Appl. Chem.* **1998**, *70*, 925−929. (i) Vrettos, J. S.;

Limburg, J.; Brudvig, G. W. *Biochim. Biophys. Acta* **2001**, *1503*, 229–245. (j) Yamanaka, S.; Isobe, H.; Kanda, K.; Saito, T.; Umena, Y.; Kawakami, K.; Shen, J. R.; Kamiya, N.; Okumura, M.; Nakamura, H.; Yamaguchi, K. *Chem. Phys. Lett.* **2011**, *511*, 138–145. (k) Kusunoki, M. *Biochim. Biophys. Acta* **2007**, *1767*, 484–492.

(3) Gao, Y.; Crabtree, R. H.; Brudvig, G. W. *Inorg. Chem.* **2012**, *51*, 4043–4050.

(4) Dismukes, G. C.; Brimblecombe, R.; Felton, G. A. N.; Prydun, R. S.; Sheats, J. E.; Spiccia, L.; Swiegers, G. F. *Acc. Chem. Res.* **2009**, *42*, 1935–1943.

(5) Wiechen, M.; Berends, H.-M.; Kurz, P. *Dalton Trans.* **2012**, *41*, 21–31.

(6) Artero, V.; Chavarot-Kerlidou, M.; Fontecave, M. *Angew. Chem., Int. Ed.* **2011**, *50*, 7238–7266.

(7) Dogutan, D. K.; McGuire, R.; Nocera, D. G. *J. Am. Chem. Soc.* **2011**, *133*, 9178–9180.

(8) Wasylenko, D. J.; Ganesamoorthy, C.; Borau-Garcia, J.; Berlinguette, C. P. *Chem. Commun.* **2011**, *47*, 4249–4251.

(9) Wasylenko, D. J.; Palmer, R. D.; Schott, E.; Berlinguette, C. P. *Chem. Commun.* **2012**, *48*, 2107–2109.

(10) Yin, Q.; Tan, J. M.; Besson, C.; Geletii, Y.; Musaev, D. G.; Kuznetsov, A. E.; Luo, Z.; Hardcastle, K. I.; Hill, C. L. *Science* **2010**, *328*, 342–345.

(11) Ellis, W. C.; McDaniel, N. D.; Bernhard, S.; Collins, T. J. *J. Am. Chem. Soc.* **2010**, *132*, 10990–10991.

(12) Lloret-Fillol, J.; Codolà, Z.; Garcia-Bosch, I.; Gómez, L.; Pla, J. J.; Costas, M. *Nat. Chem.* **2011**, *3*, 807–813.

(13) Barnett, S. M.; Goldberg, K. I.; Mayer, J. M. *Nat. Chem.* **2012**, *4*, 498–502.

(14) Zhang, M. T.; Chen, Z.; Kang, P.; Meyer, T. J. *J. Am. Chem. Soc.* **2013**, *135*, 2048–2051.

(15) Codolà, Z.; Garcia-Bosch, I.; Acuña-Parés, F.; Prat, I.; Luis, J. M.; Costas, M.; Lloret-Fillol, J. *Chem.—Eur. J.* **2013**, *19*, 8042–8047.

(16) Acuña-Parés, F.; Codolà, Z.; Costas, M.; Luis, J. M.; Lloret-Fillol, J. *Chem.—Eur. J.* **2014**, DOI: 10.1002/chem.201304367.

(17) Kasapbasi, E. E.; Whangbo, M. H. *Inorg. Chem.* **2012**, *51*, 10850–10855.

(18) Wang, D.; Que, L., Jr. *Chem. Commun.* **2013**, *49*, 10682–10684.

(19) Kundu, S.; Matito, E.; Walleck, S.; Pfaff, F. F.; Heims, F.; Rábay, B.; Luis, J. M.; Company, A.; Braun, B.; Glaser, T.; Ray, K. *Chem.—Eur. J.* **2012**, *18*, 2787–2791.

(20) Kodera, M.; Kawahara, Y.; Hitomi, Y.; Nomura, T.; Ogura, T.; Kobayashi, Y. *J. Am. Chem. Soc.* **2012**, *134* (32), 13236–13239.

(21) Becke, A. D. *J. Chem. Phys.* **1993**, *98*, 1372–1377.

(22) Becke, A. D. *J. Chem. Phys.* **1993**, *98*, 5648–5562.

(23) Lee, C. T.; Yang, W. T.; Parr, R. G. *Phys. Rev. B* **1988**, *37*, 785–789.

(24) *Gaussian 09*, Revision A.1; Frisch, M. J.; Trucks, G. W.; Schlegel, H. B.; Scuseria, G. E.; Robb, M. A.; Cheeseman, J. R.; Scalmani, G.; Barone, V.; Mennucci, B.; Petersson, G. A.; Nakatsuji, H.; Caricato, M.; Li, X.; Hratchian, H. P.; Izmaylov, A. F.; Bloino, J.; Zheng, G.; Sonnenberg, J. L.; Hada, M.; Ehara, M.; Toyota, K.; Fukuda, R.; Hasegawa, J.; Ishida, M.; Nakajima, T.; Honda, Y.; Kitao, O.; Nakai, H.; Vreven, T.; Montgomery, J. A., Jr.; Peralta, J. E.; Ogliaro, F.; Bearpark, M.; Heyd, J. J.; Brothers, E.; Kudin, K. N.; Staroverov, V. N.; Kobayashi, R.; Normand, J.; Raghavachari, K.; Rendell, A.; Burant, J. C.; Iyengar, S. S.; Tomasi, J.; Cossi, M.; Rega, N.; Millam, J. M.; Klene, M.; Knox, J. E.; Cross, J. B.; Bakken, V.; Adamo, C.; Jaramillo, J.; Gomperts, R.; Stratmann, R. E.; Yazyev, O.; Austin, A. J.; Cammi, R.; Pomelli, C.; Ochterski, J. W.; Martin, R. L.; Morokuma, K.; Zakrzewski, V. G.; Voth, G. A.; Salvador, P.; Dannenberg, J. J.; Dapprich, S.; Daniels, A. D.; Farkas, Ö.; Foresman, J. B.; Ortiz, J. V.; Cioslowski, J.; Fox, D. J. Gaussian, Inc.: Wallingford, CT, 2009.

(25) Marenich, A. V.; Cramer, C. J.; Truhlar, D. G. *J. Phys. Chem. B* **2009**, *113*, 6378–6396.

(26) Schwabe, T.; Grimme, S. *Phys. Chem. Chem. Phys.* **2007**, *9*, 3397–3406.

(27) Kelly, C. P.; Cramer, C. J.; Truhlar, D. G. *J. Phys. Chem. A* **2006**, *110*, 2493–2499.

(28) Curtiss, L. A.; Raghavachari, K.; Redfern, P. C.; Pople, J. A. *J. Chem. Phys.* **2000**, *112*, 7374–7383.

(29) Curtiss, L. A.; Raghavachari, K.; Redfern, P. C.; Pople, J. A. *J. Chem. Phys.* **1997**, *106*, 1063–1079.

(30) Winget, P.; Cramer, C. J.; Truhlar, D. G. *J. Phys. Chem. B* **2007**, *111*, 408–422.

(31) Bianco, R.; Hay, P. J.; Hynes, J. T. *J. Phys. Chem. A* **2011**, *115*, 8003–8016.

(32) Wang, L.; Wu, Q.; Voorhis, T. V. *Inorg. Chem.* **2010**, *49* (10), 4543–4553.

(33) Hirahara, M.; Ertem, M. Z.; Komi, M.; Yamasaki, H.; Cramer, C. J.; Yagi, M. *Inorg. Chem.* **2013**, *52* (11), 6354–6364.

(34) Ertem, M. Z.; Gagliardi, L.; Cramer, C. J. *Chem. Sci.* **2012**, *3*, 1293–1299.

(35) Rong-Zhen, L.; Xi-Chen, L.; Siegbahn, P. E. M. *Eur. J. Inorg. Chem.* **2014**, *14*, 728–741.

(36) Due to the extraordinary magnitude of the energy barrier and the very similar free energy between the two possible *cis*-Fe^{IV}(O)(OH$_2$)(Pytacn) tautomers (ΔG = 0.2 kcal·mol^{-1}), only one catalytic potential tautomer has been considered. We selected the most stable one, in which the Fe=O moiety is in *trans* relative position to one of the Me-substituted amines (**a**). We also selected the tautomer **a** for comparison proposals, because this is the most stable form for the *cis*-Fe^{IV}(O)(OH)(Pytacn) complex (see next section).

(37) Comba, P.; Rajaraman, G.; Rohwer, H. *Inorg. Chem.* **2007**, *46* (10), 3826–3838.

(38) Lundberg, M.; Borowski, T. *Coord. Chem. Rev.* **2013**, *257*, 277–289.

(39) Vilella, L.; Vidossich, P.; Balcells, D.; Lledós, A. *Dalton Trans.* **2011**, *40*, 11241–11247.

(40) Barone, V.; Cossi, M. *J. Phys. Chem. A* **1998**, *102*, 1995–2001.

(41) Bell, R. P. *The Proton in Chemistry*, 2nd ed.; Cornell University Press: Ithaca, NY, 1973.